On the Performance Limits of High-speed Transmission using a Single Wideband Coherent Receiver

Benedikt Geiger, *Graduate Student Member, IEEE,* Eric Sillekens, *Member, IEEE,* Filipe Ferreira, *Senior Member, IEEE,* Robert Killey, *Fellow, IEEE,* Lidia Galdino, *Senior Member, IEEE,* and Polina Bayvel, *Fellow, IEEE*

(Top-Scored)

***Abstract*—The performance of a wideband coherent receiver was investigated. The relative impact of digital pre-distortion, geometric constellation shaping and pilot sequence detection, as well as the number of sub-channels in the super-channel, on the receiver performance was explored. The detection of a net data rate of 2.36 Tb/s after 75 km transmission of a 8 $\times$ 26 GBd DP-GS-256-QAM super-channel was demonstrated using a single 110 GHz electrical bandwidth receiver. The overall improvement due to the digital pre-distortion and tailored geometric constellation shaping was 1.2 bit/4D-sym in the achievable information rate.**

***Index Terms*—optical fiber communication, high symbol rate, digital signal processing, constellation shaping**

I. Introduction

CONTINUOUS growth in digital transformation technologies has led to numerous high-data applications driving the demand for internet traffic capacity [1]. This growth in demand places a particular strain on data centre interconnect (DCI) links, and metropolitan and core networks due to the high-data applications being closer to the end user. E.g., self-driving cars and edge computing lead to increasingly high data rates being carried in the future. DCI links cover distances of typically 70-100 km and are mainly limited by the transceiver performance [2]. To cope with this exponential demand in data rate cost effectively, the throughput of the optical transceivers must be increased. The capacity C, or the maximum data rate, of a transmission system scales logarithmically with the signal-to-noise ratio (SNR) and linearly with the bandwidth B. For example, in the case of the additive white Gaussian noise (AWGN) channel,

$$C = B \cdot \log_2 (1 + \mathrm{SNR}) . \tag{1}$$

Since the capacity scales linearly with the bandwidth, one of the most straightforward approaches to increase the data rate, reduce the transceiver count, and the energy and cost per bit, is to increase the bandwidth, i.e., the symbol rate. Therefore, the challenge for future optical transmission systems is to increase the symbol rate of the transmission system while keeping the SNR constant.

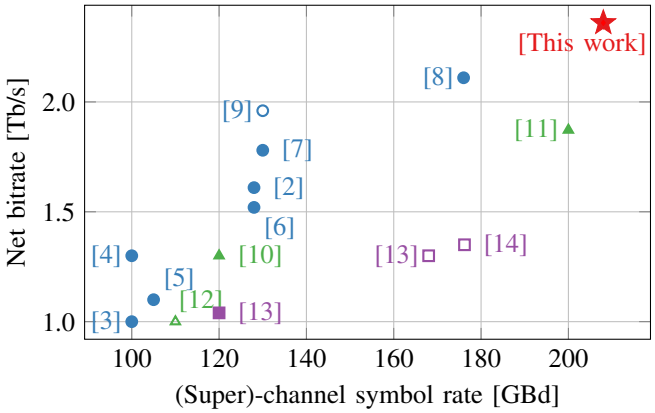

Fig. 1: Net achieved bitrates vs. (super-)channel symbol rate for recent record experiments exceeding 1 Tb/s and 100 GBd. Filled and unfilled markers refer to transmission and B2B experiments, respectively. Dots, squares, and triangles refer to digital-to-analogue converters (DACs) without interleaving, externally electrically-interleaved DACs and optically-interleaved super-channel experiments, respectively.

Fig. 1 shows previous record experiments exceeding 1 Tb/s and 100 GBd. Conventional transmission systems use a single-carrier where the transmission signal is generated by a DAC without (external) interleaving. In such transmission systems (blue dots), the symbol rate, and hence the throughput, is mainly limited by the transmitter, especially by the DACs bandwidth [6]. A close look at the results demonstrates that the symbol rate of experiments using DACs without (external) interleaving has saturated over the last few years. The

Financial support from the UK EPSRC Programme Grant TRANSNET (EP/R035342/1), Strategic Equipment Grant 'Advanced Signal Generation And Detection System For Next-generation Ultra-wideband Communication Networks'(EP/V007734/1), UKRI Future Leaders Fellowship (MR/T041218/1), Royal Academy of Engineering is gratefully acknowledged. Corning is thanked for the loan of the Corning® SMF-28® ULL optical fibre.

Benedikt Geiger was a visitor in the Optical Networks Group, Department of Electronic & Electrical Engineering, UCL (University College London), London, U.K. from the Karlsruhe Institute of Technology (KIT) in the framework of the ERASMUS+ programme. He is now with the Communications Engineering Lab (CEL), KIT. (e-mail: benedikt.geiger@kit.edu)

Eric Sillekens, Filipe Ferreira, Robert I. Killey, and Polina Bayvel are with the Optical Networks Group, UCL.

Lidia Galdino was with the Optical Networks Group, UCL and is now with Corning Optical Fiber Communications, Ewloe, U.K (e-mail: galdinol@corning.com)

Manuscript received November 29, 2022; revised March 30, 2023.

previous increases in bandwidth were based on decreasing the transistor gate length of CMOS and BiCMOS-based DACs [15]. However decreasing the transistor gate length gets increasingly more complex and expensive [16], which makes further increases in bandwidth challenging. Since a analogue-to-digital converter (ADC)s sampling process is inherently parallelisable, ADCs can be more easily parallelised than DACs. Consequently, the DACs bandwidth is currently trailing that of ADCs and there exist wideband coherent receivers with electrical bandwidths exceeding 100 GHz, leaving potential data rate unexploited. Hence, the transmitter architecture has a significant impact on the overall throughput of a transmission system. The first option to increase the symbol rate of the transmitted signal is to push the symbol rate significantly beyond the bandwidth of the transmitter. However, this is accompanied by higher inter-symbol interference (ISI) or pre-emphasis losses leading to a strong SNR degradation [7], [17] and resulting in an overall lower bit rate. A different approach to increase the symbol rate, i.e., to extend the bandwidth, is to interleave DACs either in the frequency- or time- domain [13], [14]. In these demonstrations (green triangles) up to 176.2 GBd and 1.35 Tb/s [14] have been achieved. However, the SNR and spectral efficiency degradation due to hardware limitations [14] was so significant that the maximum achieved data rates were lower than those achieved in the reported single DAC experiments. A third option to increase the symbol rate of the transmitted signal is to use an optical multi-carrier setup (purple squares), in which multiple low symbol rate signals are generated and multiplexed in the optical domain. An optical multi-carrier setup with N sub-carriers requires N DACs, N modulators and N separate modulator drivers. This could increase the complexity and cost on the transmitter side in a commercial implementation due to additionally required synchronisation. However, due to the current imbalance between transmitter and receiver bandwidth, an optical multi-carrier architecture is the only way to exploit the full bandwidth of the receiver without a very strong SNR degradation caused by the transmitter as reported in [17]. Hence, an optical multi-carrier architecture reduces the impact of the transmitter impairments while exploiting the full bandwidth of the receiver. Furthermore, this approach enables a reduction in the number of receivers required for a given throughput, reducing system complexity and cost on the receiver side. The goal of this paper is to explore this third option of generating high quality super-channels to investigate performance limits of the wideband receiver, and the potential transceiver architectures for next-generation high-speed links. The insights gained in this paper about performance limits of wideband receivers will still hold if DACs and modulators catch up in bandwidth. Obviously, in a commercial product, there will be a trade-off between cost (transmitter count) and SNR (net bitrate). Hence, a commercial product would probably use fewer optical carriers to exploit the full receiver bandwidth which reduces the SNR (net bitrate) slightly. Additionally, it must be kept in mind that the advanced digital signal processing (DSP) achieving high spectral efficiencies could introduce additional delays.

This paper extends the results reported in [18], demonstrating a 2.29 Tb/s transmission and reception using a single coherent receiver. The performance of the single- and multi-carrier transmission were compared experimentally, the transmitter and receiver noise was characterised, allowing the detailed investigation of the performance limits of wideband receiver. The first step was a single-channel investigation, in which the transmitter performance was maximised. A digital pre-distortion (DPD) was used to mitigate the roll-off and nonlinearity of the DAC and modulator, maximising the transmitted signal SNR. Geometric constellation shaping (GS) and pilot symbols were employed to maximise throughput. Extending the results for a multi-carrier transmission system, allowed the full 110 GHz bandwidth of the receiver to be exploited, with a detailed comparison of 4 and 8 sub-carriers. Finally, transmission was carried out over 75 km of single mode fibre, achieving a record net bitrate of 2.36 Tb/s using a single receiver.

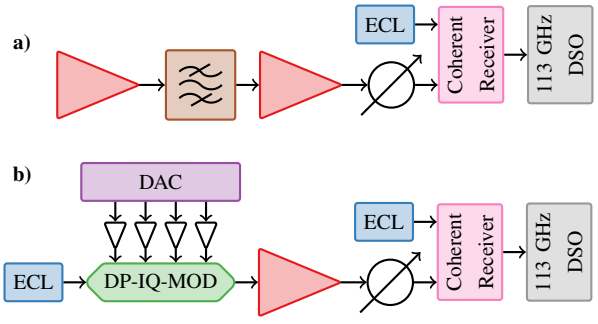

Fig. 2: Setup used to measure the transmitter and receiver transfer function: a) Receiver b) Transmitter as well as setup for single-carrier transmission

II. Transmitter and Receiver Characterisation

The overall bandwidth of the transmitter and receiver is a crucial performance characteristic when designing transceivers. This section assesses and compares the transmitter and receiver in terms of bandwidth. First, the receiver is characterised which is later used in the characterisation of the transmitter.

A. Receiver

Fig. 5 includes a photograph of the receiver: The Frauenhofer HHI coherent receiver frontend (CRF) [19] was used to convert the optical signal into the electrical domain together with the Keysight UXR [20] as digital storage oscilloscope (DSO). We used an external cavity laser (ECL) with $<$100 kHz linewidth as an local oscillator (LO). The CRF had a 3 dB bandwidth of approximately 109 GHz, with the exact value varying by approximately 1 GHz between the four individual channels. The oscilloscope operates at 256 GSa/s, has a bandwidth of 113 GHz, 10 bits of physical resolution and 5 effective number of bits (ENOB) at $\geq$ 400mV $_{\text{fs}}$ [20]. The performance of the receiver is determined by the combined frequency transfer function of the coherent receiver and the oscilloscope. There are two options to measure the combined frequency response:

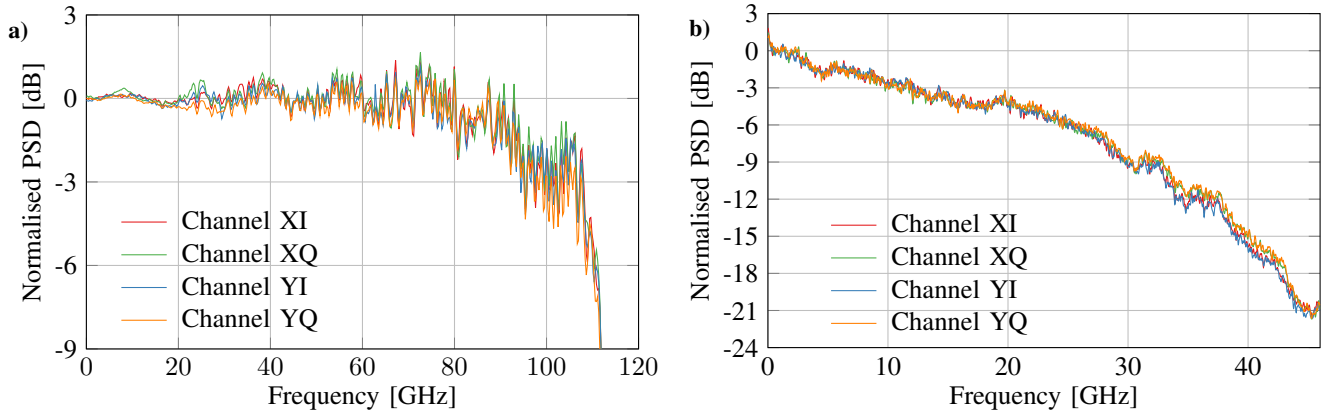

Fig. 3: (a) Receiver transfer function, (b) Combined transmitter and receiver transfer function

- Using a laser as a signal source into the coherent receiver and sweep the frequency offset between the signal and the LO or
- Using a flat broadband noise source.

We used the latter approach because, in this case, the frequency transfer function can be obtained with a single measurement. Fig. 2a shows the corresponding setup for the measurement. The measured frequency transfer function for all four channels is shown in Fig. 3a. First, it can be noted that the transfer functions of the four channels are all slightly different, and this difference can be compensated as in [21] using a linear filter to further improve performance. In addition, the transfer function is relatively flat up to 25 GHz. At frequencies above this point, ripples of up to 2 dB can be observed. Across the four channels, the average -6-dB frequency is 110.5 GHz (with contributions of 3 dB loss from the coherent receiver frontend and 3 dB from the DSO) with the exact value varying by approximately 0.5 GHz between the four individual channels with channel XI having the lowest 6-dB frequency of 110 GHz. The ripples and the roll-off of the receiver at higher frequencies limit the performance of channels, within the super-channel, that have a higher offset between the LO and the carrier. Because the roll-off and ripples are quite static, they can be mitigated. The zero-forcing equaliser would fully compensate the attenuation and would effectively reduce the ISI but would amplify the noise for the attenuated frequencies greatly. However, the overall goal is to minimise the mean squared error (MSE) and maximise the SNR as well as the throughput. Hence, the least mean square (LMS) algorithm can be used to minimise the instantaneous squared error, i.e., maximise the SNR, finding a trade-off between minimising the ISI and increasing the noise floor [6].

B. Transmitter

The transmitter setup is shown in Fig. 2b. The Keysight M8196A with a typical bandwidth of 32 GHz, with 8 physical bits resolution, 5 ENOB and a sampling rate of 92 GSa/s was used to convert the digital signal into the electrical domain. An in-depth analysis on how the DAC characteristics impact the quality of the generated transmit signal is conducted in [6], [21], [22]. The outputs of the arbitrary waveform generator (AWG) were amplified by SHF-807 linear broadband amplifiers with a bandwidth of 30 GHz. An ECL with $<$100 kHz linewidth was used as the signal carrier. The carrier was modulated by an Oclaro (now Lumentum) dual-polarisation (DP) inphase- and qaudrature- modulator (IQM) with a 3-dB bandwidth of 40 GHz. To determine the overall transfer function of the transmitter, pseudo-random data with a uniform distribution and flat power spectral density (PSD) was generated using a Mersenne twister and was loaded onto the AWG. Fig. 3b shows the combined attenuation of the transmitter and receiver. However, since the receiver's transfer function is relatively flat (compared to the transmitter) and has a maximum attenuation of up to 1 dB up to 46 GHz, the impact of the receiver roll-off in the measurement can be neglected. Therefore, Fig. 3b is a good approximation of the attenuation of the transmitter alone. Our transmitter had a single-sided 3 dB bandwidth of 12 GHz, with an attenuation of 6 dB at 25.5 GHz, and attenuated the signal at the Nyquist frequency by some 21 dB. The 6 dB bandwidth of the receiver was approximately 4.3 times larger than that of the transmitter. Hence it is clear that the transmitter is the limiting factor in the overall performance.

III. Single-carrier characterisation

This section explores the performance limits for a single-carrier transmission which is later compared to a multi-carrier transmission. Additionally, the single-carrier performance provides additional insights into the performance of our setup in terms of SNR.

A. Experimental setup and digital signal processing

For the single-carrier transmission, the same setup as for the characterisation of the transmitter was used (Fig. 2b). To mitigate the strong ripples in the receiver frequency response, first a long equaliser with 1025 taps is applied (see Sec. II-A). Furthermore, adaptive equalisers with 31-81 taps were used to boost the performance, where the actual number of taps depended on the symbol rate. Since long equalisers do not

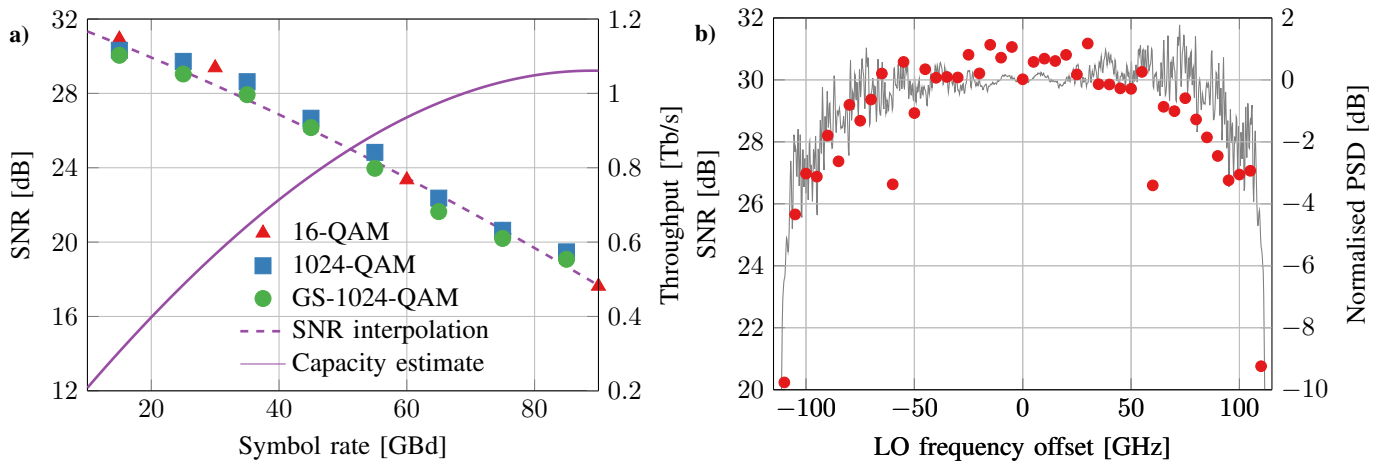

Fig. 4: Single-carrier performance in back-to-back (B2B): a) SNR over symbol rate for various modulation formats. b) SNR over the LO frequency offset for a 15 GBd signal with the transfer function of the receiver in the background. The tilt in the transfer function stems from the gain tilt of the erbium-doped fibre amplifier (EDFA) used to measure the PSD of the receiver.

reliably converge if blind DSP is used, we used a pilot-aided DSP chain following [23]. One generated transmit frame had a length of 65,536 symbols and was played periodically by the DAC. Generally, the memory length of the DAC limits the number of different transmission symbols. We used the regular square, as well as GS, constellation formats for the characterisation. The GS constellations were designed for an additive white Gaussian noise (AWGN) channel. We maximised the generalised mutual information (GMI) using the trust-region algorithm as described in [24]. The use of analytical gradients for GMI as a function of the constellation points allows the efficient optimisation of large constellation formats. Increasing the constellation size generally reduces the gap to capacity. However, due to the limited number of code rates in the family of DVB-S2X low density parity check (LDPC) codes and large gaps between the code rates for low normalised generalised mutual information values (see Sec. V-B and [25]), the constellation order was reduced to 256 for the transmission experiment. The transmitted symbols were pulse-shaped by an root raised cosine (RRC) with a roll-off factor of 1%. Finally, the transmitter impairments were mitigated using a DPD method consisting of a linear filter with 401 taps, to obtain a flat spectrum at the output of the transmitter. An arcsine transfer function with a parameter sweep-optimised clipping voltage was used to compensate for transceiver non-linearities, such as the IQ-modulator transfer function [26]. At the receiver, the DSO captured waveforms with 1,290,555 samples. First, the receiver skews were compensated and the signal was normalised. To reduce the impact of quantisation noise, the Loedwin orthogonalization was used [27]. Then the following steps were carried out for each sub-carrier: The signal was shifted by the frequency offset of the sub-carrier such that it was located at baseband (0 GHz). Next, the signal was resampled to 2 samples per symbol and the chromatic dispersion (CD) was corrected. Then, a matched RRC filter was applied to suppress the other sub-carriers. Due to a sufficiently large guardband between the sub-carriers, the other sub-carriers could be suppressed completely (see Sec. IV-A). Next, the header was used to synchronise the reference and the received signal, to obtain a rough estimate of the frequency offset and to train the first equaliser. Next, the carrier phase estimation (CPE) pilots were used to estimate the carrier phase. The equaliser pilot sequence length 2^{10} and CPE pilot insertion rate 2^6 maximising the achievable information rate (AIR) were found in a parameter sweep, leading to a pilot-overhead of 3.1% [23]. Finally, we used a k-means to maximise the SNR and finally computed the SNR, GMI, and AIR. The AIR was assessed assuming ideal forward error correction (FEC), i.e., we calculated the GMI using a Monte-Carlo integration of the received symbols [28] and subtracted the overhead associated with the pilot symbols. Practical FEC reduces the net bitrate by the coding gap and its impact is shown in Sec. V-B.

B. Symbol Rate Optimisation

The SNR performance for different symbol rates (16-quadrature amplitude modulation (QAM), 1024-QAM and GS-1024-QAM) was measured and the results are shown in Fig. 4a. For all modulation formats, the SNR decreases with increasing symbol rate. With increasing symbol rate, the attenuation of the transmitter (Fig. 3b) increases, which has to be pre-emphasised by a linear filter described in the DSP section, leading to decreased output voltage from the DAC and, consequently, a decrease in SNR. Note that the difference in SNR between the modulation formats is due to the peak-to-average power ratio (PAPR) difference between the modulation formats, with the 16-QAM having the lowest PAPR. The GS-1024-QAM has a higher PAPR than the conventional 1024-QAM resulting in a lower SNR, although despite this, the GS-QAM reduces the gap to the Shannon capacity, resulting in a higher overall throughput. Figure 4a also shows the capacity (estimated from the interpolated measured

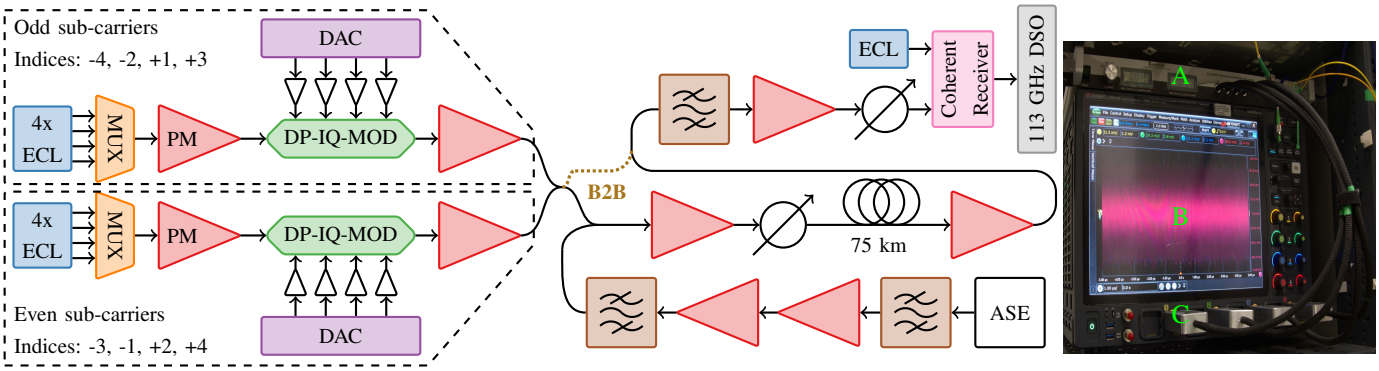

Fig. 5: Experimental setup for the multi-carrier. The photograph shows the receiver: A) Dual-Pol. 90° Optical-Hybrid. B) Keysight UXR. C) Photodiodes

SNR using Eq. 1) assuming capacity-achieving modulation. It can be seen that in the case of a single-carrier transmission, the capacity of the system increases with the symbol rate. Since the capacity increases linearly with bandwidth, and only logarithmically with SNR, the increase in bandwidth leads to a higher throughput, despite the reduction in SNR. However, it can be observed that the capacity saturates at around 90 GBd (capacity: 1.06 Tb/s). Our DAC with a maximum sampling rate of 92 GSa/s prevented us from generating symbol rates beyond 92 GBd. However, even if we were able to generate signals with a higher symbol rate, the capacity would further decrease, due to the strongly decreasing SNR. This places a limit on the maximum data rate and symbol rate which can be generated with a single-carrier architecture, which means that the full receiver bandwidth can not be exploited. This can be overcome through the use of the multi-carrier architecture, described in Sec. IV-A.

C. Impact of Frequency Offset

As a precursor for the multi-carrier transmission study, in which the carriers are multiplexed in the frequency domain, we investigated how the frequency offset between the carrier and the LO impacted the SNR. A signal with a symbol rate of 15 Gbd and a 1024-QAM was generated and the frequency offset between the LO and carrier was swept over the full bandwidth of the receiver. The resultant SNR versus the frequency offset between the carrier and the LO is shown in Fig. 4b. We chose a low symbol rate of 15 GBd because the transmitter impairments increase with the symbol rate, and we were interested in isolating performance degradation solely due to the frequency offset *at the receiver*. Since the frequency offset is achieved by detuning the LO, the noise contribution from the transmitter remains constant for all values. As expected, the SNR follows the frequency transfer function in Fig. 3a. This demonstrates that the system was mainly limited by the transfer function of the receiver. A longer equaliser length (>81 taps) helped to achieve a robust performance at high frequencies, where the frequency transfer function of the receiver has strong ripples. Overall, as can be seen in Fig. 4b, we achieved an SNR of greater than 25 dB over a range of more than 210 GHz. We attribute the drop in SNR around +/- 60 GHz to the interleaving of the UXR's internal samplers. For a high-frequency offset (>60 GHz), a reduction in the SNR was observed due to the frequency roll-off of the photodiodes in the coherent receiver and the DSO.

IV. Multi-Carrier Performance

A. Experimental setup

Next, the single-carrier setup was extended to a multi-carrier architecture. The experimental setup is shown in Fig. 5. A super-channel with 8 sub-carriers was generated by separately modulating 4 odd- and 4 even- sub-carriers. The sub-carrier lasers were free running ECLs with <100 kHz linewidth spaced at 26.5 GHz and were separately amplified by two polarisation maintaining (PM) EDFAs. This resulted in a guardband of 240 MHz and prevented the overlapping of the sub-carriers. With an optical frequency comb source, the carriers could be spaced closer, however, this could result in optical signal-to-noise ratio (OSNR) limitations [10].

The sub-carriers were modulated at 26 GBd, RRC spectrally shaped (roll-off: 0.01) GS-256-QAM. The outputs of the modulators were amplified by EDFAs and combined into a super-channel with an overall symbol rate of 8 × 26 GBd. In Sec. V-A, we compare this 8 sub-carrier setup to a setup with 4 sub-carriers. In the latter case, only four ECLs were modulated to obtain 4 × 52 GBd sub-carriers, spaced 53 GHz apart and, thus, occupying the same total bandwidth as the 8 × 26 GBd signal.

Both B2B operation, as well as transmission over fibre, were investigated. The 75 km link used the Corning® SMF-28® ULL optical fibre, with 0.156 dB/km and a total attenuation of 12.2 dB including splicing and connection losses. At the receiver, a band-pass filter was used to filter out the super-channel, which was then amplified by an EDFA and attenuated by a variable optical attenuator (VOA) to reduce signal-signal beating. Additional details to the amplified spontaneous emission (ASE) noise loading are given in Sec. V-B.

B. Impact of multiple carriers

The two overarching goals of this work were (i) to obtain insights into the interplay between transmitter and receiver

TABLE I: SNR of sub-carrier no. +1 as a function of the number of sub-carriers and resultant super-channel bandwidth.

# carrier	BW [GHz]	SNR [dB]
1	26.5	30.1
2	53	26.9
4	106	24.3
8	212	21.2

noise as well as (ii) to understand the throughput limitations of a system with a single high-bandwidth receiver. The next step was to explore the impact of the number of 26 GBd sub-carriers and the resultant super-channel bandwidth on the SNR. For this experiment, the setup was in optical B2B and the carriers were modulated with 1024-QAM. The LO and signal powers were optimised to yield the highest SNR values. We found the LO power of 15.5 dBm (the maximum output power of ECL), and the signal power of 2 dBm to maximise performance. The starting point was the transmission of a single 26 GBd sub-carrier with the resultant SNR of 30.1 dB (Tab. I). In fact, this very close to the noise limit of the AWG and DSO with an ENOB of 5. Table I shows the measured SNR of positive centre sub-carrier (+1) as a function of the number of sub-carriers. We observed that the SNR decreased by approximately 3 dB each time the number of sub-carriers was doubled. This is because the optimum signal power into the coherent receiver is independent of the number of sub-carriers. So doubling the number of sub-carriers halves the signal power per sub-carrier and, therefore, the SNR, resulting in the 3 dB decrease. Note that if optical signal power into the coherent front-end was higher, the SNR would decrease due to stronger signal-signal beating.

C. Transmitter optimization

Having understood how a multi-carrier setup impacts the centre sub-carriers, the next step was to optimise the SNR of the outer sub-carriers. Since we are interested in the performance limits of a single receiver, the resultant transmitter impairments must be minimised. In this section, we describe the application of DPD and GS and their impact on AIR improvements, since both methods have been shown to yield significant increases in data rate [2], [7], [23]. In our experiment, the sub-carriers for all channels were modulated at 256-QAM, with and without GS and with and without DPD applied. The AIR was calculated as described in Sec. III-A.

Fig. 6 shows the resultant AIR vs. sub-carrier index with and without DPD and GS in the optical B2B case where the AIR is limited by the transceiver SNR. We expected the sub-carriers with the same index, e.g. +1 and -1 to have the same performance but it was noted that the performance strongly depended on whether or not the carrier was suppressed by adjusting the bias applied to the IQM. Generally, the AIR was governed by a combination of the transmitter and receiver noise

$$\frac{1}{\mathrm{SNR}_{\mathrm{TRx}}(f)} = \frac{1}{\mathrm{SNR}_{\mathrm{Tx}}(f)} + \frac{1}{\mathrm{SNR}_{\mathrm{Rx}}(f)}. \quad (2)$$

Since the 8 sub-carrier signal was generated by two AWGs, both the odd-channels and the even channels carried the same data and had similar quality - any variation in the AIR between channels was caused by the receiver.

Although we expected the performance of the sub-carriers to follow the shape of Fig. 3a, we observed that especially the sub-channels +/- 2/3 were degraded more strongly than expected. In comparison to the sweep of the single-channel we carried out in the earlier experiment, an additional sub-channel at the image frequency leads to additional interference and performance degradation.

Initially, we used the DPD described in Sec. III-A to mitigate transmitter impairments enabling an AIR improvement of (0.87 bit/4D-sym) on average, as can be seen in Fig. 6.

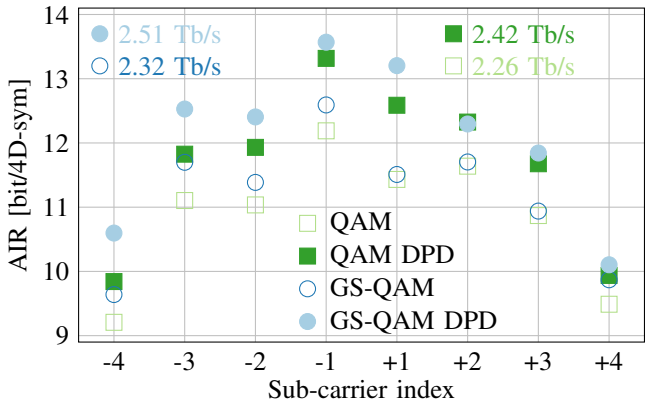

Fig. 6: Transmitter maximisation: AIR improvement due to DPD and GS. Filled and unfilled markers refer to with and w/o DPD, respectively. Dots and squares refer to GS-QAM and QAM, respectively.

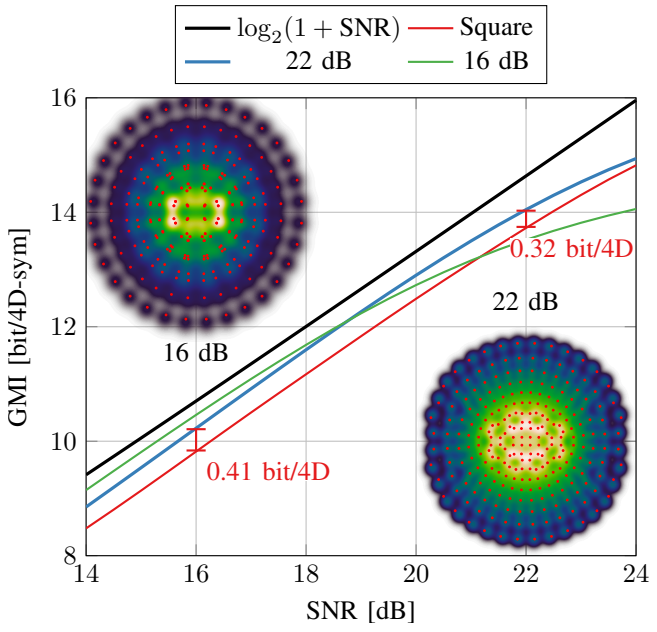

Fig. 7: The geometrically shaped constellations optimised for 16 and 22 dB with the GMI for an AWGN channel showing the gap to capacity. The insets show the constellations designed for 16 and 22 dB SNR.

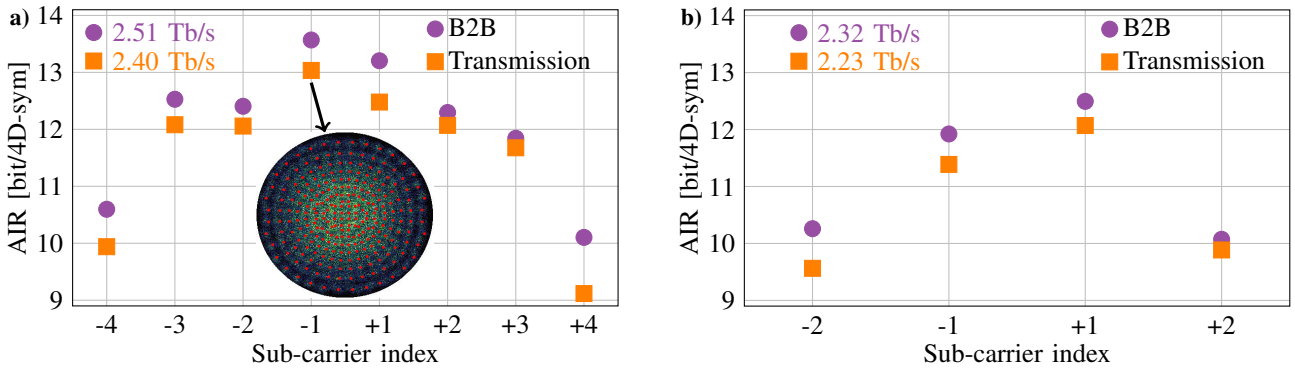

Fig. 8: AIR in B2B case and after 75km transmission for (a) 8x26 GBd sub-carrier setup and (b) 4x52 GBd sub-carrier setup. The inset shows the transmitted and received constellation diagram of sub-carrier -1 after 75 km transmission.

It can be seen that the performance improvement decreases for outer carriers: For the centre and outer sub-carriers, the AIR improvements were 1.23 bit/4D-sym and 0.57 bit/4D-sym, respectively. The performance of the outer sub-carriers was mainly dominated by the (low) receiver SNR reducing the relative importance of the transmitter impairments. The improvement in performance due to transmitter DPD of the centre sub-carriers is more significant, since the receiver attenuation is lower at low frequencies.

Secondly, a GS constellation design, aimed at closing the shaping gap to the AWGN capacity and increasing the AIR as described in Sec. III-A was applied at the transmitter. A gradient descent algorithm was used to find the constellation coordinates (Fig. 7) which maximise the GMI for a 256-ary constellation, tailored to the AWGN channel with the highest observed SNR [24], [29]. This was 22 dB for the centre sub-carriers. This would incur a smaller penalty than using the constellation designed for 16 dB SNR. Note that due to the bulk modulation of odd- and even- sub-carriers it was not possible to tailor the GS for each individual sub-carrier and it was tailored to the sub-carriers with the highest observed SNR, which are the centre sub-carriers. In contrast to the DPD, the rate gain due to GS is approximately constant over the sub-carriers with an average of 0.33 bit/4D-sym, where for the AWGN channel we predicted (obtained) a 0.32 (0.33) and 0.41 (0.43) bit/4D-sym increase for the centre channels and outer channels, respectively. Overall, DPD and GS enabled a B2B AIR of 2.51 Tb/s, with the DPD contributing 180 Gb/s and the GS 70 Gb/s, on average.

V. Transmission Experiments

Transmission was carried out in two steps. First, two single super-channel configurations with 8 $\times$ 26 GBd and 4 $\times$ 52 GBd were compared before moving on to wavelength division multiplexing (WDM).

A. Comparison between 4 and 8 sub-carriers

Fig. 8a compares, first, the AIR between a setup with 4 and 8 sub-carriers and, additionally, the AIR between B2B operation and transmission over 75 km Corning® SMF-28® ULL fibre. We expected the 4 sub-carrier setup to have the same throughput as the 8 sub-carrier setup. However, the transceiver performance depends on the transmitter and receiver noise contributions. Since the allocated bandwidth was the same for both setups, the overall receiver noise contribution was the same for both cases. Tab. I shows that each time the number of sub-carriers was doubled, the receiver SNR decreased by 3 dB. However, Fig. 4a shows a SNR degradation of more than 3 dB each time the symbol rate is doubled. E.g., doubling the symbol rate from 26 GBd to 52 GBd led to a reduction in SNR of approximately 4.3 dB. Using fewer sub-carriers requires the use of a higher symbol rate per sub-carrier to achieve the same overall bandwidth. A higher symbol rate results in higher transmit signal impairments, leading to a trade-off between transmitter count and signal quality. Since the 8 $\times$ 26 GBd architecture outperformed the 4 $\times$ 52 GBd architecture (Fig. 8a and 8b), the 8 $\times$ 26 GBd architecture was used in the WDM transmission experiment.

The transmission over a 75 km SMF link on the AIR was investigated next and the results are shown in Fig. 8a which compares the AIR, calculated from the GMI, between B2B operation and transmission over 75 km SMF. The optimal launch power of 5 dBm was determined in a parameter sweep. Only a small degradation was observed, compared to the B2B case, because the performance was largely limited by the transceiver SNR rather than the OSNR limitation and fibre non-linearity for DCI distances [15]. This differs from the experiments reported in [10] in which an optical comb generator was used and the setup was OSNR limited, highlighting the advantage of free-running ECL.

B. WDM transmission experiment

The final experiment was carried out to investigate the WDM transmission performance of 14 super-channels occupying a total bandwidth of 2.97 THz (each of the 14 super-channels was 8 $\times$ 26 GBd). A spectrally-shaped amplified spontaneous emission (SS-ASE) noise source covering the 1539 nm to 1563 nm wavelength band was used to emulate the other 13 C-band interfering super-channels [30]. The minimum and maximum wavelengths were limited by the EDFA bandwidth and the tuneable ECL. A notch was carved into the SS-ASE, into which the super-channel-under-test was inserted,

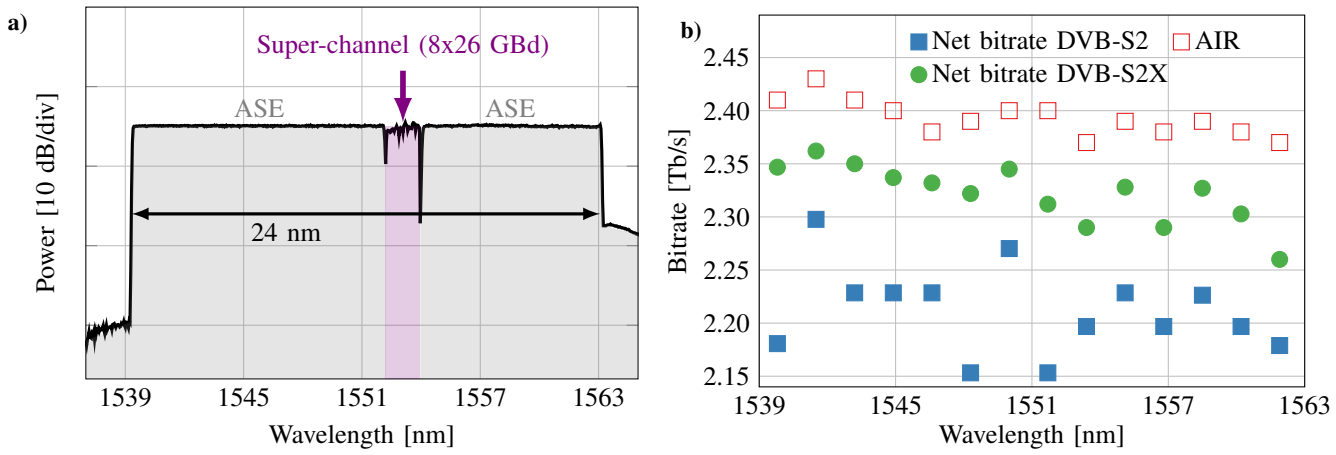

Fig. 9: WDM experiment: Wavelength dependence across the entire C-band. The data points give the wavelength of the LO. (a) Spectrum (b) AIR and net bitrate

with its power controlled to ensure its power spectral density matched that of the SS-ASE noise (Fig. 9a). The spectrum of the WDM signal was measured and is shown in Fig. 9a. A launch power of 14 dBm was selected (corresponding to 2.5 dBm and -6.5 dBm per super-channel and per sub-carrier, respectively) maximising the AIR; this was determined by sweeping the launch power. In the following experiment, the position of the super-channel was swept over the C-band and the received signal was FEC decoded to determine the wavelength dependence of the AIR and net bitrate across the entire C-band. Fig. 9b shows the resultant AIR and net bitrate values for the 14 super-channels after transmission over the 75 km link. We observed that the AIR decreased slightly with wavelength, due to the gain tilt of the amplifier in the noise loading stage, leading to 33.5 Tb/s AIR over the C-band. In comparison to the transmission of a single super-channel without ASE, described in the previous subsection and carried out around 1550 nm, a significant performance degradation was not observed. In both cases the AIR was 2.40 Tb/s. Hence, we can deduce that even at the increased optical power levels in the fibre in WDM case, the performance is mainly limited by the transceiver noise rather than fibre non-linearities over this short distance. Despite the lower per channel power compared to the single super-channel case, we are not OSNR limited because the transceiver noise is dominant, compared to the ASE noise. In [18], we used the family of DVB-S2 LDPC codes and an outer BCH (30832,30592) code to FEC decode the data. Since the family of DVB-S2 LDPC codes has only 11 codes, this resulted in an quite high average coding gap of $\frac{30.96\ \text{Tb/s}}{33.50\ \text{Tb/s}}$ = 7.58% and a high variance in the net bitrate. Therefore, we use in this paper the family of DVB-S2X LDPC codes [25] with smaller gaps between the code rates achieving a net bitrate of 2.36 Tb/s for the best performing channel and an net bitrate of 32.5 Tb/s over the C-band.

C. Gap to the Ideal Receiver

To put the achieved performance into perspective, we compare the results with an ideal receiver. The limit of the system is the quantisation noise of the DSO in the receiver. If we use the formula for converting 5 bit ENOB to SNR [31] with the added correction for the PAPR difference between the signal and the sine wave with which the PAPR was measured:

$$\text{SNR} = \underbrace{20\log_{10}(5)}_{\text{ENOB}} + \underbrace{20\log_{10}\left(\frac{\sqrt{12}}{2}\right)}_{\text{quantisation noise}} - \underbrace{12}_{\text{PAPR}} = 22.87\,\text{dB}. \tag{3}$$

The value of 12 dB for the PAPR was chosen because the signal after dispersion appears almost Gaussian distributed and this was confirmed by measuring the PAPR of received signals experimentally, which were in the range of 12.6 and 15.0 dB.

The resulting capacity of the 5 ENOB and 110 GHz receiver is $C = 2B \cdot \log_2(1 + \text{SNR}) = 3.34$ Tb/s. The achieved 2.51 Tb/s is 75.2 % of the theoretical maximum. This difference can be accounted for by the transmitter, optical noise, the coherent receiver and the photodiodes.

VI. Conclusion

We investigated the performance limits on the data rate of next-generation >100 GHz receivers with a super-channel symbol rate of 208 GBd. Using an optical multi-carrier architecture, we experimentally demonstrated an AIR of 2.51 Tb/s in optical B2B, an AIR and net bitrate of 2.43 Tb/s and 2.36 Tb/s over a 75 km ultra-low-loss fibre, respectively. In addition, the multi-carrier architecture allowed the exploration of the transceiver noise contributions together with a comparison between a 4 × 52 GBd vs 8 × 26 GBd setup.

To the best of our knowledge, the reported results represent the highest data rate received with a single coherent receiver. The previous record net bitrate achieved using a single receiver has been exceeded by 250 Gb/s [8]. The record was enabled by the multi-carrier architecture generating multiple high quality sub-carriers exploiting the 110 GHz electrical bandwidth of the receiver. Additionally, long filter and pilot-based DSP were used to combat the ripples in the frequency response of the

receiver. A DPD, and GS increased the SNR and reduced the gap to the Shannon capacity enabling an AIR improvement of 170 Gb/s and 75 Gb/s on average, respectively, with less than 25% gap to capacity for an ideal receiver.

REFERENCES

[1] P. Bayvel, R. Maher, T. Xu, G. Liga, N. A. Shevchenko, D. Lavery, A. Alvarado, and R. I. Killey, "Maximizing the Optical Network Capacity," *Philosophical Transactions of the Royal Society A: Mathematical, Physical and Engineering Sciences*, vol. 374, no. 2062, 2016.

[2] V. Bajaj, F. Buchali, M. Chagnon, S. Wahls, and V. Aref, "Single-Channel 1.61 Tb/s Optical Coherent Transmission Enabled by Neural Network-Based Digital Pre-Distortion," in *2020 European Conference on Optical Communications (ECOC)*, Dec. 2020, pp. 1–4.

[3] K. Schuh, F. Buchali, W. Idler, T. A. Eriksson, L. Schmalen, W. Templ, L. Altenhain, U. Dümler, R. Schmid, M. Möller, and K. Engenhardt, "Single Carrier 1.2 Tbit/s Transmission over 300 Km with PM-64 QAM at 100 GBaud," in *2017 Optical Fiber Communications Conference and Exhibition (OFC)*, Mar. 2017, pp. 1–3.

[4] F. Buchali, K. Schuh, R. Dischler, M. Chagnon, V. Aref, H. Buelow, Q. Hu, F. Pulka, M. Frascolla, E. Alhammadi, A. Samhan, I. Younis, M. El-Zonkoli, and P. Winzer, "1.3-Tb/s Single-Channel and 50.8-Tb/s WDM Transmission over Field-Deployed Fiber," in *45th European Conference on Optical Communication (ECOC 2019)*, Sep. 2019, pp. 1–4.

[5] F. Buchali, V. Lauinger, M. Chagnon, K. Schuh, and V. Aref, "1.1 Tb/s/λat 9.8 Bit/s/Hz DWDM Transmission over DCI Distances Supported by CMOS DACs," in *Optical Fiber Communication Conference : 8-12 March 2020, San Diego, California, United States*, 2020, p. 3.

[6] F. Buchali, V. Aref, R. Dischler, M. Chagnon, K. Schuh, H. Hettrich, A. Bielik, L. Altenhain, M. Guntermann, R. Schmid, and M. Möller, "128 GSa/s SiGe DAC Implementation Enabling 1.52 Tb/s Single Carrier Transmission," *Journal of Lightwave Technology*, vol. 39, no. 3, pp. 763–770, 2021.

[7] F. Pittalà, R.-P. Braun, G. Böcherer, P. Schulte, M. Schaedler, S. Bettelli, S. Calabrò, M. Kuschnerov, A. Gladisch, F.-J. Westphal, C. Xie, R. Chen, Q. Wang, and B. Zheng, "1.71 Tb/s Single-Channel and 56.51 Tb/s DWDM Transmission Over 96.5 km Field-Deployed SSMF," *IEEE Photonics Technology Letters*, vol. 34, no. 3, pp. 157–160, Feb. 2022.

[8] M. Nakamura, M. Nagatani, T. Jyo, F. Hamaoka, M. Mutoh, Y. Shiratori, H. Wakita, T. Kobayashi, H. Takahashi, and Y. Miyamoto, "Over 2-Tb/s Net Bitrate Single-carrier Transmission Based on >130-GHz-Bandwidth InP-DHBT Baseband Amplifier Module," in *2022 European Conference on Optical Communication (ECOC)*, 2022, pp. 1–4.

[9] M. Xu, Y. Zhu, F. Pittalà, J. Tang, M. He, W. C. Ng, J. Wang, Z. Ruan, X. Tang, M. Kuschnerov, L. Liu, S. Yu, B. Zheng, and X. Cai, "Dual-polarization Thin-film Lithium Niobate In-phase Quadrature Modulators for Terabit-per-second Transmission," *Optica*, vol. 9, no. 1, pp. 61–62, Jan 2022. [Online]. Available: https://opg.optica.org/optica/abstract.cfm?URI=optica-9-1-61

[10] R. Maher, A. Alvarado, D. Lavery, and P. Bayvel, "Increasing the Information Rates of Optical Communications via Coded Modulation: A Study of Transceiver Performance," *Scientific Reports*, vol. 6, no. 1, p. 21278, 2016.

[11] S. T. Le, V. Aref, and X. Chen, "2 Tb/s Single-ended Coherent Receiver," in *2021 European Conference on Optical Communication (ECOC)*, 2021, pp. 1–4.

[12] D. S. Millar, R. Maher, D. Lavery, T. Koike-Akino, M. Pajovic, A. Alvarado, M. Paskov, K. Kojima, K. Parsons, B. C. Thomsen, S. J. Savory, and P. Bayvel, "Detection of a 1 Tb/s Superchannel with a Single Coherent Receiver," in *2015 European Conference on Optical Communication (ECOC)*, 2015, pp. 1–3.

[13] M. Nakamura, F. Hamaoka, M. Nagatani, H. Yamazaki, T. Kobayashi, A. Matsushita, S. Okamoto, H. Wakita, H. Nosaka, and Y. Miyamoto, "1.04 Tbps/Carrier Probabilistically Shaped PDM-64QAM WDM Transmission Over 240 km Based on Electrical Spectrum Synthesis," *2019 Optical Fiber Communications Conference and Exhibition (OFC)*, 2019.

[14] X. Chen, S. Chandrasekhar, G. Raybon, S. Olsson, J. Cho, A. Adamiecki, and P. Winzer, "Generation and Intradyne Detection of Single-Wavelength 1.61-Tb/s Using an All-Electronic Digital Band Interleaved Transmitter," in *2018 Optical Fiber Communications Conference and Exposition (OFC)*, 2018, pp. 1–3.

[15] F. Buchali, V. Lauinger, M. Chagnon, K. Schuh, and V. Aref, "CMOS DAC Supported 1.1 Tb/s/λDWDM Transmission at 9.8 bit/s/Hz Over DCI Distances," *Journal of Lightwave Technology*, vol. 39, no. 4, pp. 1171–1178, 2021.

[16] T. Drenski and J. C. Rasmussen, "Adc & DAC — Technology Trends and Steps to Overcome Current Limitations," in *2018 Optical Fiber Communications Conference and Exposition (OFC)*, 2018, pp. 1–3.

[17] H. Mardoyan, S. Almonacil, F. Jorge, F. Pittala, M. Xu, B. Krueger, F. Blache, B. Duval, L. Chen, Y. Yan, X. Ye, A. Ghazisaeidi, S. Rimpf, Y. Zhu, J. Wang, M. Goix, Z. Hu, M. Duthoit, M. Grün, X. Cai, and J. Renaudier, "First 260-GBd Single-Carrier Coherent Transmission over 100 km Distance Based on Novel Arbitrary Waveform Generator and Thin-Film Lithium Niobate I/Q Modulator," in *2022 European Conference on Optical Communication (ECOC)*, 2022, pp. 1–4.

[18] B. Geiger, E. Sillekens, F. Ferreira, R. Killey, L. Galdino, and P. Bayvel, "Record 2.29 Tb/s GS-256QAM Transmission using a Single Receiver," in *2022 European Conference on Optical Communication (ECOC)*, 2022, pp. 1–3.

[19] *100 GHz Coherent Receiver Frontend*, https://www.hhi.fraunhofer.de/en/departments/pn/products-and-solutions/coherent-receiver-frontend.html, Frauenhofer HHI, 2022.

[20] *Infiniium UXR-Series Oscilloscopes: The most advanced oscilloscope on the planet*, https://www.keysight.com/de/de/assets/7018-06242/data-sheets/5992-3132.pdf, Keysight Technologies, 2023.

[21] M. Torbatian, D. Lavery, M. Osman, D. Yao, D. S. Millar, Y. Gao, A. Kakkar, Z. A. El-Sahn, C. Doggart, A. E. Morra, N. Abughalieh, S. Yang, X. Chen, R. Maher, H. Sun, K.-T. Wu, and P. Kandappan, "Performance Oriented DSP for Flexible Long Haul Coherent Transmission," *Journal of Lightwave Technology*, vol. 40, no. 5, pp. 1256–1272, 2022.

[22] W. Kester, *The Data Conversion Handbook*. Newnes, 2004.

[23] Y. Wakayama, T. Gerard, E. Sillekens, L. Galdino, D. Lavery, R. I. Killey, and P. Bayvel, "2048-QAM transmission at 15 GBd over 100 km using geometric constellation shaping," *Opt. Express*, no. 12, pp. 18 743–18 759, 2021.

[24] E. Sillekens, G. Liga, D. Lavery, P. Bayvel, and R. I. Killey, "High-Cardinality Geometrical Constellation Shaping for the Nonlinear Fibre Channel," *arXiv*, 2022.

[25] "Digital Video Broadcasting (DVB); Second generation framing structure, channel coding and modulation systems for Broadcasting, Interactive Services, News Gathering and other broadband satellite applications; Part 2: DVB-S2 Extensions (DVB-S2X)," European Telecommunications Standards Institute (ETSI), Sophia-Antipolis, France, Standard, Jul. 2021.

[26] J. Song, C. Häger, J. Schröder, A. G. I. Amat, and H. Wymeersch, "Model-Based End-to-End Learning for WDM Systems With Transceiver Hardware Impairments," *IEEE Journal of Selected Topics in Quantum Electronics*, vol. 28, no. 4, pp. 1–14, 2022.

[27] P.-O. Löwdin, "On the Non-Orthogonality Problem Connected with the Use of Atomic Wave Functions in the Theory of Molecules and Crystals," *The Journal of Chemical Physics*, vol. 18, no. 3, p. 365, 1950, publisher: American Institute of PhysicsAIP.

[28] A. Alvarado, T. Fehenberger, B. Chen, and F. M. J. Willems, "Achievable Information Rates for Fiber Optics: Applications and Computations," *Journal of Lightwave Technology*, vol. 36, no. 2, pp. 424–439, 2018.

[29] E. Sillekens, D. Semrau, D. Lavery, P. Bayvel, and R. Killey, "Experimental Demonstration of Geometrically-Shaped Constellations Tailored to the Nonlinear Fibre Channel," in *2018 European Conference on Optical Communication (ECOC)*, 2018, pp. 1–3.

[30] D. J. Elson, G. Saavedra, K. Shi, D. Semrau, L. Galdino, R. Killey, B. C. Thomsen, and P. Bayvel, "Investigation of Bandwidth Loading in Optical Fibre Transmission Using Amplified Spontaneous Emission Noise," *Optics Express*, vol. 25, no. 16, pp. 19 529–19 537, 2017.

[31] W. Kester. Taking the Mystery out of the Infamous Formula, "SNR = 6.02N + 1.76dB," and Why You Should Care. [Online]. Available: https://www.analog.com/media/en/training-seminars/tutorials/MT-001.pdf